ChemPubSoc Europe

DOI: 10.1002/cplu.201402032

Keeping Nanoparticles Fully Functional: Long-Term Storage and Alteration of Magnetite

Marc Widdrat,[a] Monika Kumari,[b] Éva Tompa,[c] Mihály Pósfai,[c] Ann M. Hirt,[b] and Damien Faivre*[a]

Magnetite is an iron oxide found in rocks. Its magnetic properties are used for paleoclimatic reconstructions. It can also be synthesized in the laboratory to exploit its magnetic properties for bio- and nanotechnological applications. However, although the magnetic properties depend on particle size in a well-understood manner, they also depend on the structure of the oxide, because magnetite oxidizes to maghemite under environmental conditions. The dynamics of this process have not been well described. Here, a study of the alteration of magnetite particles of different sizes as a function of their storage conditions is presented. Smaller nanoparticles are shown to oxidize more rapidly than larger ones, and that the lower the storage temperature, the lower the measured oxidation. In addition, the magnetic properties of the altered particles are not decreased dramatically, thus suggesting that this alteration will not impact the use of such nanoparticles as medical carriers.

Introduction

Magnetite (Fe_3O_4) is a naturally occurring magnetic iron oxide mineral, which has numerous bio- and nanotechnological applications.[1,2] The magnetic properties of magnetite nanoparticles are typically used in magnetic inks, storage media, or biomedical applications such as magnetic resonance imaging (MRI), hyperthermia treatment, or drug delivery.[1,2] Furthermore, the magnetic properties of iron oxides in general and of magnetite in particular are used in geo- and paleomagnetism, because these minerals preserve the main vectors of the Earth's magnetization,[3] and can therefore be used to reconstruct past continental positioning and climates.[4,5]

The magnetic properties of magnetite nanoparticles typically depend on their size, morphology, and assembly. Particles smaller than about 30 nm are so-called superparamagnetic (SP),[6] that is, they only have a measurable magnetic signal if placed in an external magnetic field. Larger nanoparticles have intrinsic and permanent magnetic moments. Particles with isometric shapes from 25–30 nm to about 80–100 nm fall within the stable single domain (SSD) category. Larger particles are called multi-domain (MD), in which several magnetic domains coexist, reducing the magnetostatic energy.[7] The effects of size and morphology have been studied in the past.[8,9] However, the magnetic properties of magnetite nanoparticles also depend on oxidative processes, as these usually result in structural changes. Hence, to define storage conditions to keep drugs in a functional state and to better understand the mechanism of rock magnetization acquisition and evolution by environmental magnetite nanoparticles, we must understand how magnetite nanocrystals evolve upon exposure to atmospheric oxygen. Such a process indeed reflects the diagenetic processes observed on the Earth's surface or if nanoparticles are stored in aqueous solutions, in which maghemite (γ-Fe_2O_3) is the natural weathering product of magnetite formed as oxygen causes the oxidation of the mixed Fe^{II}/Fe^{III} oxide to the pure Fe^{III} oxide.[3]

The crystal structure of maghemite is very similar to that of magnetite. Both oxides crystallize in the inverse spinel group with a cubic unit cell ($a_{magnetite} = 0.83969$ nm[10] and $a_{maghemite} = 0.83419$ nm). The unit cell of magnetite contains 32 cubic closely packed O^{2-} ions; eight of the tetrahedral positions are filled with Fe^{3+} ions, and half of the octahedral positions are filled with eight Fe^{3+} ions and eight Fe^{2+} ions. The tetrahedrally and octahedrally bound iron ions form two different sublattices. These sublattices have antiparallel spins and a different net value, which is why magnetite is ferrimagnetic. In the oxidation process, the unit cell undergoes a partial removal of iron to compensate the positive charges. The unit cell of ma-

[a] M. Widdrat, Dr. D. Faivre
Department of Biomaterials
Max Planck Institute of Colloids and Interfaces
Science Park Golm, 14424 Potsdam (Germany)
Fax: (+49) 0331/567-9402
E-mail: damien.faivre@mpikg.mpg.de

[b] M. Kumari, A. M. Hirt
Institute of Geophysics, ETH-Zürich
Sonneggstrasse 5, CH-8092 Zürich (Switzerland)

[c] É. Tompa, M. Pósfai
Department of Earth and Environmental Sciences, University of Pannonia
Egyetem u. 10, H8200 Veszprém (Hungary)

Supporting information for this article is available on the WWW under http://dx.doi.org/10.1002/cplu.201402032.

This article is part of the "Early Career Series". To view the complete series, visit: http://chempluschem.org/earlycareer.

ghemite contains 32 O^{2-} and 21 1/3 Fe^{3+} ions with the same crystalline structure as magnetite, but has vacancies in the crystal lattice.[11,12] Maghemite also has two antiparallel sublattices with a nonzero net magnetic moment, and therefore, is also ferrimagnetic. The change in the crystal lattice causes a small decrease in the saturation magnetization compared with magnetite, but it is often difficult to distinguish the two minerals on the basis of their magnetic properties.[3,6] Hematite (α-Fe_2O_3) is the most thermodynamically stable iron oxide phase under ambient conditions. Although the transformational change of maghemite to hematite usually occurs at high temperatures, Colombo et al. showed that lattice imperfections can lead to partial hematite formation.[13] Stacking faults in the inverse spinel structures can behave like nuclei of hematite. This process appears favorably for larger particles owing to the higher lattice strain. Hematite has a hexagonal unit cell with six formula units (18 O^{2-} ions and 12 Fe^{3+} ions), and the lattice parameters are $a = 0.5034$ nm and $c = 1.3752$ nm. Hematite is antiferromagnetic with a weak ferrimagnetic defect moment, and is therefore magnetically distinguishable from magnetite and maghemite.[3]

Several techniques have been used to study the structural and magnetic properties of magnetite/maghemite mixtures. X-ray absorption spectroscopy (XAS) was used to quantify the oxidation states of iron in minerals or to study the local order around the iron sites.[14–16] Furthermore, the stoichiometric ratio has been studied through acidic dissolution, Mössbauer spectroscopy, powder-X-ray diffraction (XRD),[17] and X-ray magnetic circular dichroism (XMCD) techniques.[18] Particle size has been shown to play an important role in changing the stoichiometric ratio, and also influences the magnetic properties.[19,20]

However, a quantitative study of the evolution of the structural and magnetic properties of magnetic nanoparticles upon aging in an aqueous solution is still lacking. We present here a study in which magnetite nanoparticles of different sizes (SSD) are stored in aqueous solutions either at room temperature under an air (a.t.) or argon (a.t.+Ar) atmosphere, in a fridge (4 °C), or in a freezer (−20 °C) over a period of 18 months. We study the structural properties of the nanoparticles by synchrotron-based X-ray diffraction and transmission electron microscopy, and analyze their bulk magnetic properties. We show that, not surprisingly, the smaller particles have a higher oxidized volume fraction than the larger particles, and that the lower the temperature, the less the magnetic particles are oxidized. Because the magnetic properties of magnetite and maghemite are similar, the magnetic parameters are less sensitive to oxidation.

Results and Discussion

We synthesized magnetite through a procedure based on a modified version of the coprecipitation method.[21] The setup enabled the formation of size-controlled nanoparticles beyond the SSD threshold.[21] The particles were kept in solution after synthesis and stored under four different sets of conditions: at room temperature (a.t.); at room temperature with the headspace flushed with Argon (a.t.+Ar); in the fridge (4 °C); and in the freezer (−20 °C). We chose these conditions because besides the use of argon, which only reflects storage under inert conditions, these are common ways of storing goods, not only in science but also in medicine, industry, and so on. We analyzed a set of four samples with different particle sizes. The samples were studied over a period of 18 months and subjected to six analyses during this interval.

The initial stage

We investigated four samples of different particle sizes for this study (see Table 1). Figure 1 presents a summary of the properties of sample 121 at the initial stage (for the other samples see the Supporting Information). XRD confirms the presence of crystalline magnetite in all the samples (Figure 1a). The mean diameter (d_{total}) and lattice parameter (a) were calculated from the (311) peak, which is the most intensive peak in the X-ray diagram of magnetite. Transmission electron microscopy shows the presence of aggregated electron-dense magnetite nanoparticles (Figure 1b). The average particle size is in the magnetic single domain range, although the size distribution is broad and may include superparamagnetic or multidomain grains. A more precise determination of the size distribution from TEM is not possible owing to the high aggregation tendency of particles larger than a few nanometers. A study by Baumgartner et al. showed that small magnetite nanoparticles exhibit a self-similar growth behavior,[22] which in our case leads us to the conclusion that all the samples have similar size distributions. Variation in the magnetic properties is caused by both the variation in the particle size distributions and aggregation (Table 1). The saturation magnetization M_S and the saturation remanence M_{RS} are in the range of magnetite, but aggregation will depress M_{RS}. The hysteresis loop is open and the isothermal remanent magnetization curve is saturated between 200 and 230 mT (Figure 1c,d). Sample 124, with the smallest particle size, shows the lowest M_S and M_{RS}, which would be expected if some oxidation to maghemite or hematite has already occurred. M_S for sample 125 is too high and may suggest the presence of another iron species, be-

Table 1. Particle size and magnetic properties of initial samples: saturation magnetization (M_S), saturation remanent magnetization (M_{RS}), coercivity (H_C), and coercivity of the remanence (H_{CR}).

Parameters	Sample			
	121	123	125	124
average size ($d_{initial}$) [nm]	63	52	50	33
size distribution [nm]	10–300	10–100	10–90	10–100
M_S [A m^2 kg^{-1}]	87.2	83.81	105.5	75.29
M_{RS} [A m^2 kg^{-1}]	13.4	15.22	17.61	8.81
M_{RS}/M_S	0.15	0.18	0.17	0.12
H_C [mT]	8.6	10.4	9.9	6.2
H_{CR} [mT]	17.6	17.8	17.7	12.0
H_{CR}/H_C	2.0	1.7	1.8	1.9

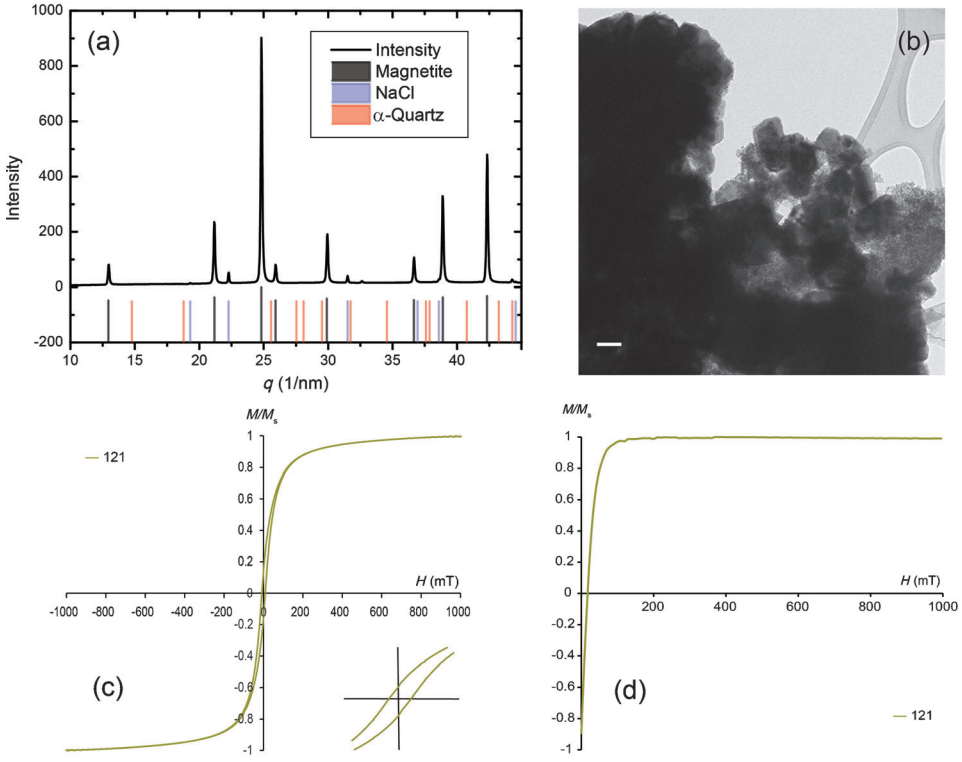

Figure 1. Sample 121: a) XRD diagram showing typical magnetite/maghemite patterns. In addition, NaCl (side product of the synthesis) and α-quartz (reference material) are observed. b) TEM image showing aggregate nanoparticles (scale bar: 100 nm). c) Hysteresis loop with expanded view to identify M_R and H_C, and d) isothermal remanent magnetization (IRM) curve.

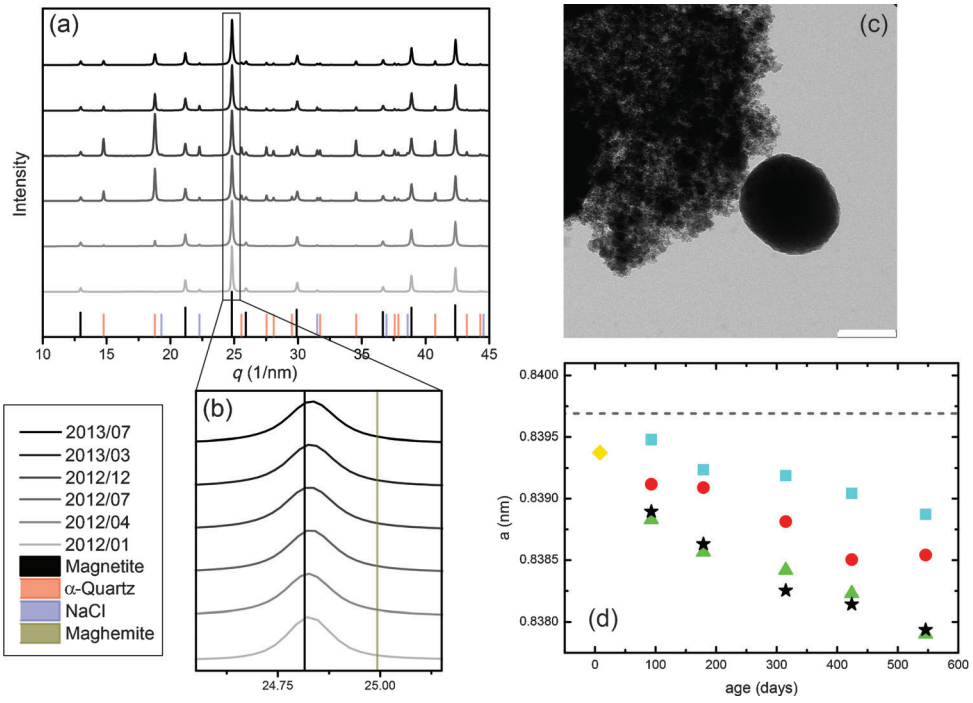

Figure 2. Summary of structural properties observed for sample 121. a) XRD diagram for the sample at different stages of the alteration study, with b) expanded view of the (311) peak. c) TEM image of the sample in the final state (scale bar: 100 nm), and d) time-resolved evolution of the lattice parameter for the different storage conditions (initial state shown by yellow diamonds, −20 °C by blue squares, 4 °C by red circles, a.t. by green triangles, and a.t. + Ar by black stars).

cause the measured lattice parameter is also larger than for pure stoichiometric magnetite.

Structural evolution

Figure 2 presents a summary of the evolution of sample 121. XRD shows typical magnetite/maghemite patterns over the entire time period (Figure 2a), and there is no indication that another oxide structure has formed. Closer inspection of the 311 peak reveals a continuous shift from the ideal magnetite peak position with time (Figure 2b). TEM investigation shows highly aggregated nanoparticles and polycrystalline sphere-like structures of magnetite/maghemite (Figure 2c). In addition, in sample 121, supercell reflections indicate the presence of both vacancy-ordered maghemite structures and a surface layer with a structure similar to that of feroxyhyte, as described recently by Rečnik et al.[23] (for more information, see the Supporting Information).The lattice parameter can be calculated from the peak position (for more information, see the Supporting Information), and the evolution of the lattice parameter can be seen in Figure 2d.

Initially all samples have the lattice parameter $a_{average} = 0.8395 \pm 0.0005$ nm (sample 121 is representative in Figure 2 with $a = 0.83937$), which is close to that of magnetite. We observe a decrease in the lattice parameter over time for all samples and all storage conditions (for more information, see the Supporting Information), which indicates a continuous oxidation toward maghemite. More specifically, the samples stored at room temperature have a smaller lattice parameter a than the sample stored in the freezer (Table 2). The samples stored in the fridge fall between these two groups. The decrease in a can be attrib-

Table 2. Change in the lattice parameter, *a*, oxidation state, *z*, and particle core (d_{core}), and shell thickness (d_{layer}) for different storage conditions as a function of alteration time for sample 121.

Conditions	Age [days]	*a* [nm]	*z*	d_{total} [nm]	d_{core} [nm]	d_{layer} [nm]
−20 °C	8	0.8394	0.0575	63.00	61.77	0.62
	93	0.8395	0.0384	–	62.19	0.41
	179	0.8392	0.0827	–	61.22	0.89
	315	0.8392	0.0913	–	61.03	0.99
	424	0.8390	0.1177	–	60.43	1.29
	546	0.8389	0.1485	–	59.72	1.64
4 °C	93	0.8391	0.1042	–	60.74	1.13
	179	0.8391	0.1091	–	60.62	1.19
	315	0.8388	0.1594	–	59.46	1.77
	424	0.8385	0.2155	–	58.11	2.45
	546	0.8385	0.2089	–	58.27	2.37
a.t.	93	0.8388	0.1564	–	59.53	1.74
	179	0.8386	0.2042	–	58.38	2.31
	315	0.8384	0.2312	–	57.72	2.64
	424	0.8382	0.2656	–	56.84	3.08
	546	0.8379	0.3250	–	55.27	3.87
a.t. + Ar	93	0.8389	0.1447	–	59.81	1.60
	179	0.8386	0.1926	–	58.67	2.17
	315	0.8383	0.2613	–	56.96	3.02
	424	0.8381	0.2817	–	56.43	3.29
	546	0.8379	0.3189	–	55.43	3.79

uted to a more pronounced oxidized state; therefore, samples stored at room temperature oxidize faster than those kept at lower temperatures. In addition, the samples flushed with argon and sealed with Parafilm did not show different behavior from that stored in air. This suggests that the argon atmosphere was not stable over time, and that oxygen penetrated the sample nearly as efficiently as in the case of the non-flushed samples. Furthermore, we observe a peak broadening as a function of aging. This peak broadening can either be correlated with a decrease in particle size as the particles are altered (a shrinkage that cannot be observed by TEM), or more probably, reflects the oxidation process with the formation of a small maghemite peak on the edge of the magnetite peak, effectively resulting in a broadening of the measured peak.

The size of the sample also plays a role in the alteration (Figure 3b). The smallest particles (sample 124) with an average diameter of 33 nm oxidize more readily, as seen from the decrease in *a* compared with the other samples with an average diameter of 50 to 63 nm.

We introduce an oxidation parameter to describe the measured lattice parameter by the ratio between the maghemite and magnetite contents. If we assume a mixture of magnetite and maghemite and their respective lattice parameter *a*, an oxidation parameter, *z*, can be defined by Equation (1), in which $a_{maghemite} < a_{experimental} < a_{magnetite}$. The oxidation can also be expressed as a percentage [Eq. (1)]. For example, the initial value of sample 121 ($a_{initial} = 0.8394$ nm) yields $z = 0.0575$, which means that 5.75% of the sample was oxidized at the initial stage. After 18 months, the degree of oxidation increases to 15% in the freezer, 21% in the fridge, and 32% for particles stored under ambient conditions (Table 1 for sample 121 and Tables S2–S4 of the Supporting Information for samples 123, 124, and 125).

$$z = \frac{a_{magnetite} - a_{experimental}}{a_{magnetite} - a_{maghemite}} \quad (1)$$

$$Oxidation(\%) = z * 100\% \quad (2)$$

For the maghemite/magnetite system, we introduce an idealized model based on a core–shell structure to depict the situation schematically (Figure 4).[3,24] With the assumption of a spherical shape for the particles, oxidation occurs at the surface so that a layer of maghemite is obtained around the magnetite core. Further oxidation causes growth of the maghemite layer and shrinkage of the inner core. Both the core diameter (d_{core}) and layer thickness (d_{layer}) can be calculated from the oxidation parameter (*z*) and the mean diameter (d_{total}), as shown in the [Eqs. (3)–(6)]. For sample 121, we have an initial maghemite layer of 0.62 nm, which is about 2% of the particle radius ($r_{total} = 31.5$ nm). The mean diameter of the particles is assumed to be constant (for more information, see the Supporting Information) and set to the initial value (Table 1). After 18 months, the maghemite layer increases to 1.64 nm if stored in the freezer, 2.37 nm in the fridge, and 3.83 nm under ambient con-

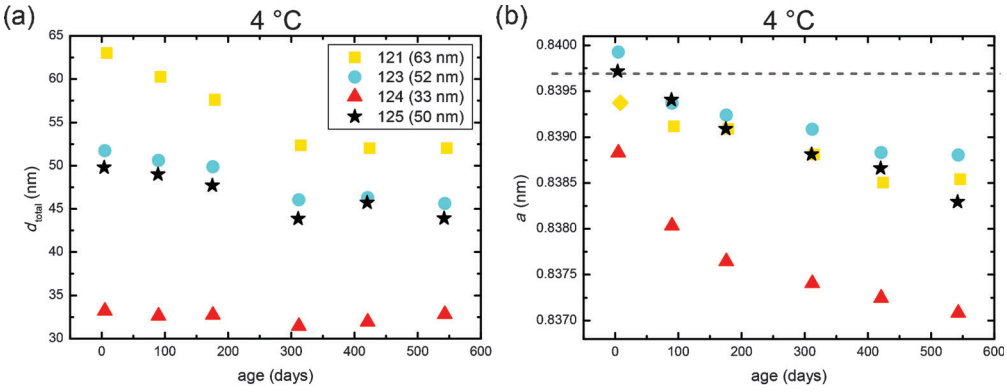

Figure 3. Change in a) particle size d_{total} and b) lattice parameter *a* as a function of aging for all four samples stored in the fridge at 4 °C. Sample 124, $d_{total} = 33$ nm, is shown by red triangles; sample 121, $d_{total} = 63$ nm, by yellow squares; sample 123, $d_{total} = 52$ nm, by blue circles, and sample 125, $d_{total} = 50$ nm, by black stars. The dashed gray line indicates the lattice parameter of magnetite.

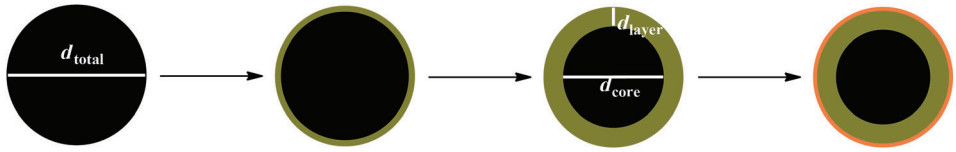

Figure 4. Oxidation model for the path from magnetite (black) to maghemite (dark yellow) and hematite (orange); a magnetite sphere is partially oxidized on the surface, and the growth proceeds inwards at the expense of the magnetite core; a possible transformation of maghemite to hematite could occur on the surface.

ditions (Table 2 for sample 121 and Tables S2–S4 for the samples 123, 124, and 125).

$$V_{core} = (1-z)V_{total} \text{with} V = \frac{1}{6}\pi d^3 \quad (3)$$

$$d_{core} = \sqrt[3]{(1-z)d_{total}^3} \quad (4)$$

$$V_{layer} = V_{total} - V_{core} = zV_{total} \quad (5)$$

$$d_{layer} = \frac{1}{2}(d_{total} - d_{core}) = \frac{1}{2}\left(d_{total} - \sqrt[3]{(1-z)d_{total}^3}\right) \quad (6)$$

Figure 5 shows the schematic development of the maghemite layer over time for all the different storage conditions. The size dependence—the small particles oxidize faster than the larger ones under any conditions—can be seen again. For particles stored at 4 °C and under ambient conditions, we observe a nonlinear growth (Figure 5 b–d). We assume that the outward migration of the Fe^{II} ions is the rate-limiting step, as diffusion in the solid phase is significantly slower than in the gaseous phase. Oxidation is fastest in the first 100–200 days of storage, independent of the particle size, for samples stored at room temperature or in the fridge. Subsequently, the amount of oxidation in the samples increases more slowly. The particles stored at −20 °C show a more complex oxidation behavior initially, but all the samples become more oxidized with time (Figure 5 a). It should be noted that the water around the particles in the freezer is frozen in this state, and this could have an influence on the initial oxidation process. In general, smaller particles oxidize faster at the beginning, but at some point they reach the same rate of oxidation as the larger particles.

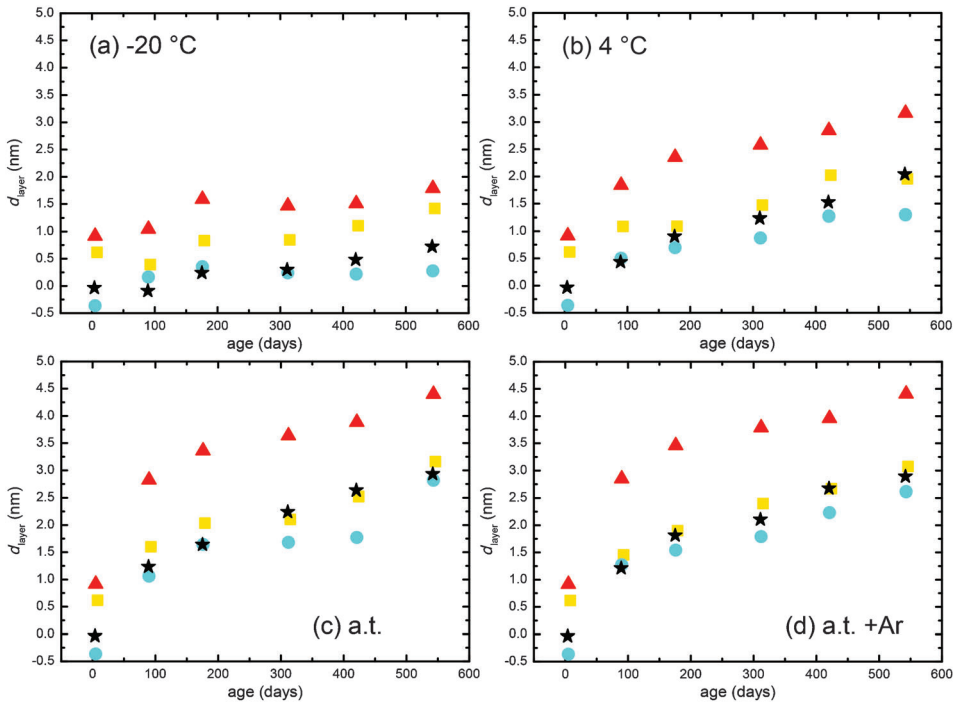

Figure 5. The evolution of the maghemite layer at −20 °C (a), 4 °C (b), a.t. (c) and a.t. + Ar (d) for samples 121 (yellow squares, d_{total} = 63 nm), 123 (blue circles, d_{total} = 52 nm), 124 (red triangles, d_{total} = 33 nm) and 125 (black stars, d_{total} = 50 nm).

Evolution of magnetic properties

Magnetic parameters are sensitive for detecting the presence of hematite. In particular, there will be an increase in H_C and H_{CR} owing to the higher coercivity of hematite and a decrease in M_{RS} and M_S owing to its lower saturation magnetization. Because the magnetic properties of magnetite and maghemite are very similar, it is more difficult to detect the oxidation of magnetite to maghemite through magnetic methods. First-order reversal curve (FORC) distributions do not show a large difference, but they are broader in general for samples under ambient temperature and under Ar at ambient temperature (Figure 6). It should be noted, however, that because of the variable but small concentration for individual samples, the signal-to-noise ratio is high.

The magnetic parameters M_{RS}/M_S and H_{CR}/H_C listed in Table 3 show that the samples stored in the freezer are most similar to the initial values in samples 123, 124, and 125. The samples show no systematic difference in H_{CP} and $H_{Cmedian}$ under different storage conditions, except for the samples stored in the freezer. The samples stored in the freezer show a lower $H_{Cmedian}$, so freezing may lead to a narrower coercivity distribution. Although none of these changes are large, there are slightly higher magnetization ratios and an increase in H_C or H_{CP} if these samples are stored under ambient conditions. The change is most noticeable in sample 124 with the smallest particle size. Sample 121

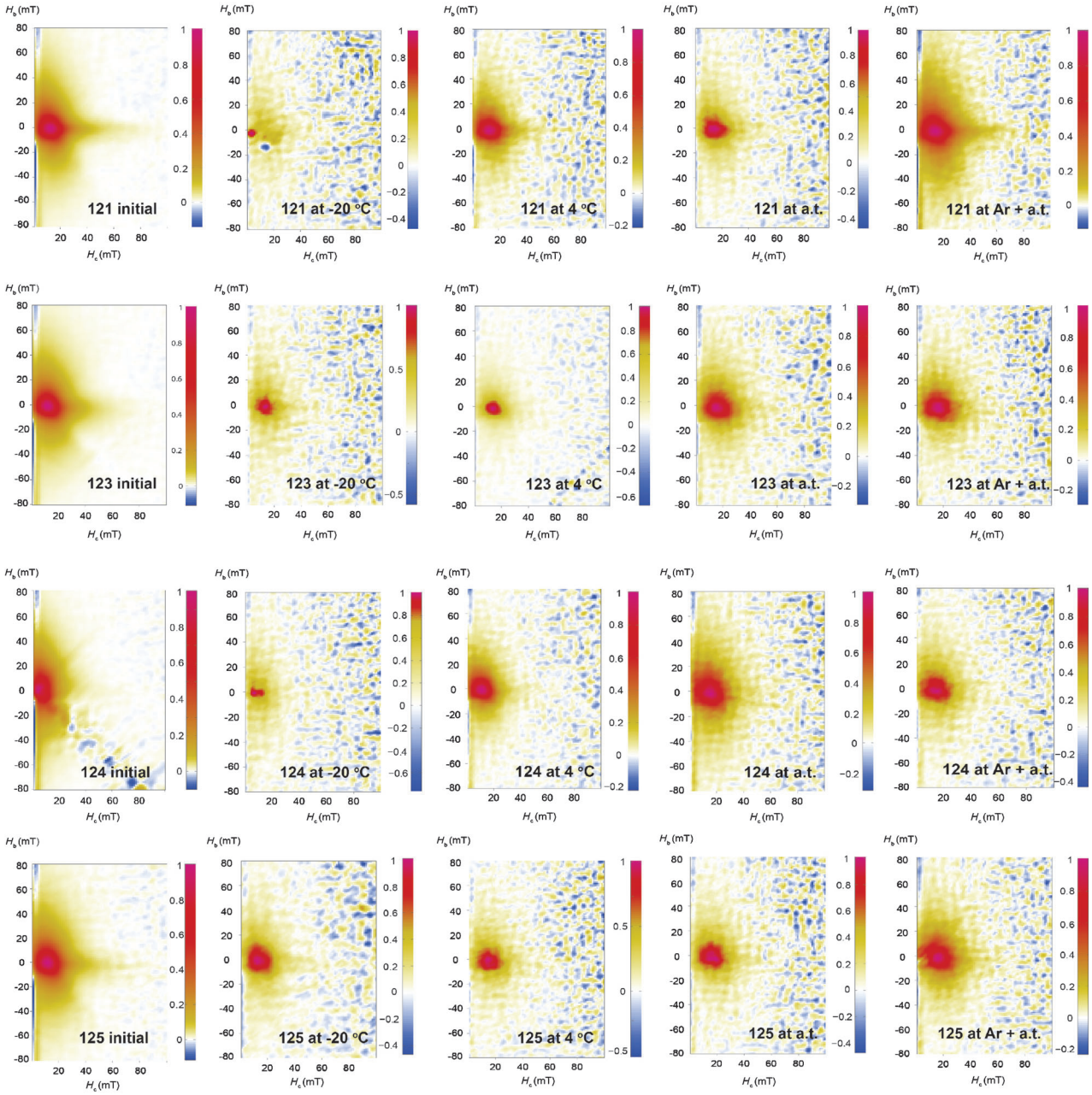

Figure 6. FORC distributions of samples 121, 123, 124, and 125 under different storage conditions. Smoothing factor, SF = 2 for all FORC diagrams.

shows a similar trend between the initial magnetic properties and the samples stored at ambient temperature or 4 °C. Storage in the freezer, however, leads to the formation of hematite, as seen from the increase in H_C/H_{CR}. A hematite shell will decrease the core diameter of some magnetite so that it is superparamagnetic, which leads to pinching of the hysteresis loop and nonsaturation of the isothermal remanent magnetization (IRM) in the maximum applied field (Figure 7).

Conclusion

We have analyzed the structural and magnetic properties of magnetite nanoparticles stored under different conditions to estimate the material quality and to study its alteration as a function of aging. High-resolution X-ray diffraction enabled us to distinguish between magnetite and maghemite, and thereby, to estimate the oxidation process by observing the evolution of the lattice parameter under different storage conditions over 18 months. We confirmed experimentally that, as expected, smaller particles, which have a higher surface-to-volume ratio, oxidize faster than larger particles, and lower temperatures cause less oxidation. We introduced an oxidation parameter and used it to describe the growth of the maghemite layer around the magnetite core.

In addition, we have analyzed the magnetic properties of the same set of samples. The magnetic properties of the sam-

Table 3. Summary of magnetic parameters for the four samples under different storage conditions initially and after 18 months.

Sample	M_{RS}/M_S	H_{CR}/H_C	H_{CP} [mT]	$H_{Cmedian}$ [mT]	$H_{B1/2}$ [mT]
121					
Initial	0.15	2.0	13	31.6	25
−20 °C	0.12	3.2	4	23.8	8
4 °C	0.20	1.8	14	31.7	29
a.t.	0.16	1.9	14	33.2	25
a.t. + Ar	0.19	1.9	15	31.5	25
123					
Initial	0.18	1.7	13	30.6	23
−20 °C	0.18	1.9	13	25.2	25
4 °C	0.23	1.7	16	31.1	25
a.t.	0.21	1.8	16	32.8	25
a.t. + Ar	0.24	1.6	17	28.8	25
124					
Initial	0.12	1.9	5	29.8	26
−20 °C	0.13	1.9	10	16.5	30
4 °C	0.20	1.7	11	30.1	30
a.t.	0.20	1.8	16	30.7	30
a.t. + Ar	0.19	1.8	15	32.8	30
125					
Initial	0.17	1.8	12	30.6	25
−20 °C	0.18	1.9	13	23.2	25
4 °C	0.18	1.9	16	34.9	25
a.t.	0.20	1.8	16	30.3	25
a.t. + Ar	0.23	1.7	17	32.8	25

ples do not vary greatly with aging, and thus, with increasing degree of oxidation, probably because the magnetic properties of magnetite and maghemite are similar. The magnetization and coercivity ratios are typically closer to the initial values for the samples stored in the freezer. Again, as expected, the change in these ratios is the largest in sample 124 with the smallest particle diameter, reflecting its higher degree of oxidation.

Our study therefore shows that if an oxidation layer is formed on the surface of magnetite nanoparticles, as measured by the decrease in the lattice parameter, this layer does not impact the magnetic properties of the samples dramatically. In turn, if magnetic properties are necessary, for example, in biomedical applications such as drug targeting, the particles are not altered dramatically over a period of more than a year.

Experimental Section

Magnetite synthesis

Magnetite was synthesized through the coprecipitation method controlled by a titration system (Metrohm, 776 Dosimat and 719 S Titrino). Fe^{II}/Fe^{III} chloride solution (1 M, Fe^{II}/Fe^{III} = 1:2) was added at 1 μL min^{-1} to a total volume of 10 mL. The pH and temperature were kept constant during the process (pH 9 ± 0.4 with 1 M NaOH; T = 5 ± 0.1 °C (124), 15 ± 0.1 °C (125), 20 ± 0.1 °C (123) and 25 ± 0.1 °C (121)). All solutions were degassed before use, and the system was kept under a nitrogen atmosphere during the synthesis. Four different storage conditions were chosen for each sample: −20 °C, 4 °C, ambient temperature (a.t.), and ambient temperature under an Ar atmosphere (a.t. + Ar; the sample was degassed with Ar after the synthesis and after each opening for sample preparation for the next measurement).

X-ray diffraction

Sample preparation was performed in a similar manner regardless of the storage conditions. Briefly, all aliquots were dried under atmospheric conditions together with an α-quartz standard[25] on a Kapton thin film and measured within the next day. In this way, if any oxidation should occur during this short period of time as compared with the testing period, this process would be of similar magnitude for all samples.

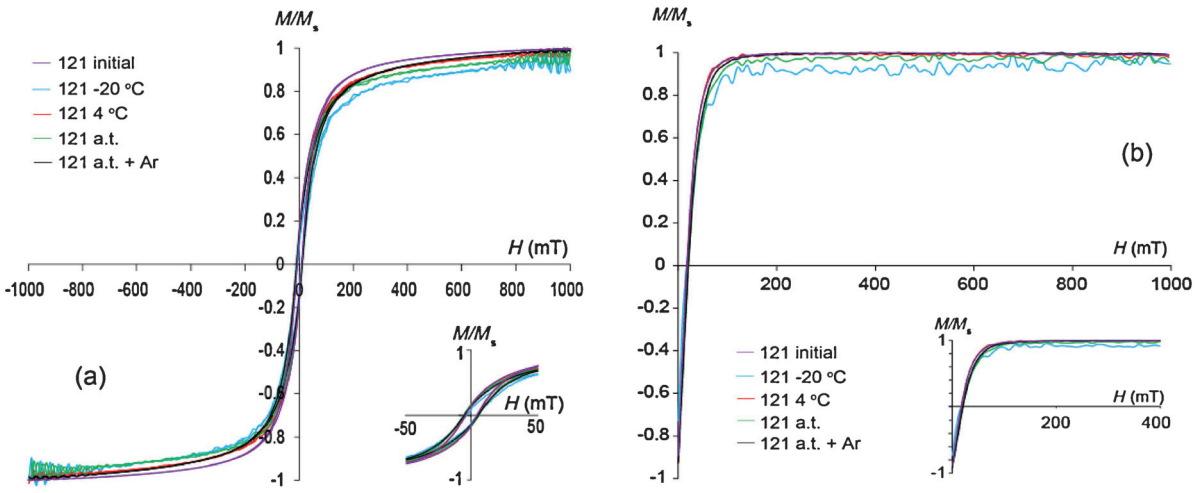

Figure 7. Initial and final states of sample 121. a) Hysteresis loops with expanded view to identify M_R and H_C, and b) isothermal remanent magnetization (IRM) curve.

Measurements were performed in transmission with a 100 μm beam of wavelength $\lambda \approx 0.82656$ Å at the μ-Spot beam line, BESSY II, Berlin. Fit2D[26] and AutoFit[27] were used to calculate the exact wavelength of the beam and the exact position of the (311) peak of the sample for subsequent calculation of the lattice parameter. The size was determined by fitting the (311) peak by Scherrer analysis with a pseudo-Voigt function and instrumental broadening correction.[28]

Transmission electron microscopy

Transmission electron microscopy images were obtained to characterize the physical dimensions, morphologies, structures, and compositions of the nanoparticles. The early state (04/2012) was documented with JEOL 2000FX (Arizona State University, USA) and Philips CM20 (Institute of Technical Physics and Materials Science, Hungary) instruments, and the final state (01/2014) with a Zeiss 912 Omega instrument (Max Planck Institute of Colloids and Interfaces, Germany) and a JEOL 3010 electron microscope (Institute of Technical Physics and Materials Science).

Magnetic measurements

Magnetic measurements were performed on the samples that were dried on a filter paper at ambient temperature in the fume hood. The sample powders were then immobilized by placing them into gently pressed gel caps. Note that all the samples were subjected to the same sample preparation. The magnetic properties of the samples were characterized by room-temperature hysteresis loops, the acquisition of an isothermal remanent magnetization (IRM), and first-order reversal curves (FORCs). All measurements were performed with a Princeton Measurements Corporation (PCM) vibrating sample magnetometer (VSM). Hysteresis loops were measured between +1 and −1 T with 100 ms averaging time to characterize the saturation magnetization (M_S), saturation remanent magnetization (M_{RS}) and coercivity (H_C) of the bulk sample. The IRM acquired in a backfield was obtained by first inducing M_{RS} at 1 T, and then demagnetizing in a backfield until −1 T to obtain the coercivity of the remanence (H_{CR}). FORC analysis was used to quantify the coercivity distribution (H_{CD}), peak coercivity (H_{CP}) of the particles, and the degree of magnetic interactions ($H_{B1/2}$),[29–34] defined from the distribution of the interaction field as the full width at half the maximum value. This value provides a measure of the differences in the amount of particle interaction between the different samples and different storage methods. Each FORC was measured by first saturating the sample with a positive applied field of 1 T and then ramping down the field to a reversal field, then measuring the magnetization as the field increases from the reversal field back to positive saturation. A series of 140 FORCs with a field spacing of 2.6 mT was used for the analysis. FORC data were transformed into FORC diagrams using M. Winklhofer MATLAB code[35] with a smoothing factor (SF) of two for all samples.

Acknowledgements

Financial support to D.F. from the European Research Council (Starting Grant MB2 no. 256915), and from the Max Planck Society is acknowledged. A.M.H., É.T., M.P., and D.F. are supported by the European Union (Project Bio2MaN4MRI no. 245542). We thank Chenghao Li and Stefan Siegel for technical assistance at the μ-SPOT Beamline (BESSY Synchrotron, Berlin).

Keywords: hematite · iron · magnetic properties · magnetite · nanoparticles

[1] S. Laurent, D. Forge, M. Port, A. Roch, C. Robic, L. Vander Elst, R. N. Muller, *Chem. Rev.* **2008**, *108*, 2064 – 2110.
[2] R. A. Frimpong, J. Z. Hilt, *Nanomedicine* **2010**, *5*, 1401 – 1414.
[3] R. M. Cornell, U. Schwertmann, *The Iron Oxides: Structure, Properties, Reactions, Occurences and Uses, 2nd ed.*, Wiley-VCH, Weinheim, **2003**.
[4] R. F. Butler, *Paleomagnetism: Magnetic Domains to Geologic Terranes*, University of Arizona, Tucson, **1998**.
[5] L. Tauxe, S. K. Banerjee, R. F. Butler, R. van der Voo, *Essentials of Paleomagnetism*, University of California Press, Berkeley, **2009**.
[6] D. J. Dunlop, Ö Özdemir, *Rock Magnetism: Fundamentials and Frontiers*, Cambridge University Press, New York, **1997**.
[7] R. F. Butler, S. K. Banerjee, *J. Geophys. Res.* **1975**, *80*, 4049 – 4058.
[8] W. Williams, A. R. Muxworthy, G. A. Paterson, *J. Geophys. Res.* **2006**, *111*, B12S13.
[9] A. R. Muxworthy, W. Williams, *J. Geophys. Res.* **2006**, *111*, B12S12.
[10] M. E. Fleet, *Acta Cryst.* **1981**, *B37*, 917 – 920.
[11] K. J. Gallagher, W. Feitknecht, U. Mannweiler, *Nature* **1968**, *217*, 1118 – 1121.
[12] W. Feitknecht, K. J. Gallagher, *Nature* **1970**, *228*, 548 – 549.
[13] U. Colombo, G. Fagherazzi, F. Gazzarrini, G. Lanzavecchia, G. Sironi, *Nature* **1968**, *219*, 1036 – 1037.
[14] P. A. van Aken, B. Liebscher, V. J. Styrsa, *Phys. Chem. Miner.* **1998**, *25*, 323 – 327.
[15] G. A. Waychunas, M. J. Apted, G. E. Brown, *Phys. Chem. Miner.* **1983**, *10*, 1 – 9.
[16] J. P. Crocombette, M. Pollak, F. Jollet, N. Thromat, M. Gautier-Soyer, *Phys. Rev. B Condens. Matter.* **1995**, *52*, 3143 – 3150.
[17] C. A. Gorski, M. M. Scherer, *Am. Mineral.* **2010**, *95*, 1017 – 1026.
[18] S. Staniland, B. Ward, A. Harrison, G. van der Laan, N. Telling, *Proc. Natl. Acad. Sci. USA* **2007**, *104*, 19524 – 19528.
[19] A. G. Roca, J. F. Marco, M. D. P. Morales, C. J. Serna, *J. Phys. Chem. C* **2007**, *111*, 18577 – 18584.
[20] J. Santoyo Salazar, L. Perez, O. de Abril, L. T. Phuoc, D. Ihiawakrim, M. Vazquez, J.-M. Greneche, S. Begin-Colin, G. Pourroy, *Chem. Mater.* **2011**, *23*, 1379 – 1386.
[21] J. Baumgartner, L. Bertinetti, M. Widdrat, A. M. Hirt, D. Faivre, *PLoS One* **2013**, *8*, e57070.
[22] J. Baumgartner, A. Dey, P. H. Bomans, C. Le Coadou, P. Fratzl, N. A. Sommerdijk, D. Faivre, *Nat. Mater.* **2013**, *12*, 310 – 314.
[23] A. Rečnik, I. Nyirő-Kósa, I. Dódony, M. Pósfai, *CrystEngComm* **2013**, *15*, 7539 – 7549.
[24] R. Frison, G. Cernuto, A. Cervellino, O. Zaharko, G. Maria Colonna, A. Guagliardi, N. Masciocchi, *Chem. Mater.* **2013**, *25*, 4820 – 4827.
[25] Standard Reference Material 1878a. *Natl. Inst. Stand. Technol.* **2005**, *1* – 4.
[26] A. Hammersley, Fit2D, http://www.esrf.eu/computing/scientific/FIT2D/.
[27] C. Lee, AutoFit.
[28] A. Fischer, M. Schmitz, B. Aichmayer, P. Fratzl, D. Faivre, *J. R. Soc. Interface* **2011**, *8*, 1011 – 1018.
[29] C. Pike, A. Fernandez, *J. Appl. Phys.* **1999**, *85*, 6668 – 6676.
[30] C. R. Pike, A. P. Roberts, K. L. Verosub, *Geophys. J. Int.* **2001**, *145*, 721 – 730.
[31] A. P. Roberts, C. R. Pike, K. L. Verosub, *J. Geophys. Res.* **2000**, *105*, 28461 – 28475.
[32] A. R. Muxworthy, J. G. King, D. Heslop, *J. Geophys. Res.* **2005**, *110*, B01105.

[33] A. R. Muxworthy, A. P. Roberts, in *First-order Reversal Curve (FORC) Diagrams in Encyclopedia of Geomagnetism and Paleomagnetism* (Eds.: D. Gubbins, E. Herrero-Bervera), Springer, Dordrecht, **2007**, pp. 2266 – 272.
[34] C. Carvallo, A. R. Muxworthy, D. J. Dunlop, *Phys. Earth Planet. Inter.* **2006**, *154*, 308 – 322.
[35] M. Winklhofer, G. T. Zimanyi, *J. Appl. Phys.* **2006**, *99*, 08E710.

Received: February 24, 2014
Revised: June 18, 2014
Published online on July 17, 2014